

Optimizing Heating Efficiency of Hyperthermia: Specific Loss Power of Magnetic Sphere Composed of Superparamagnetic Nanoparticles

Malka N. Halgamuge^{1, *} and Tao Song^{2, 3}

Abstract—Magnetic nanoparticle (MNP) based thermal therapies have shown importance in clinical applications. However, it lacks a compromise between its robustness and limitations. We developed theoretical strategies to enhance the heating efficiency, which could be utilized in thermal therapies and calculated parameter dependence for superparamagnetic MNPs (approximative ellipsoid-shaped) within a sphere-shaped ball. Then we calculated specific loss power (SLP) for magnetic particles in a magnetic ball. The dependency of features of the nanoparticles (such as mean particle size, a number of particles, frequency and amplitude of the exposed field, relaxation time, and volume gap between particles and a sphere-shaped ball) on the SLP or the heating effect in superparamagnetic MNPs was analyzed. In this study, optimal parameter values were calculated using Kneedle Algorithm as the optimization technique to represent the accurate heating efficiency. The influence of a number of particles in a sphere-shaped ball shows that SLP of magnetic particles increases with the increasing number of particles (N); however, after $N = 10$ particles, the SLP increment is insignificant. The most remarkable result arising from this analysis is that when particles are closer together (less volume gap of a sphere-shaped ball), high SLP is found for the same number of particles. This model also predicts that the frequency dependency on the SLP is negligible when the frequency is higher than 10 kHz depending on the size of a sphere-shaped ball and nanoparticle parameters. This analysis has shown that the SLP of MNPs, in a sphere-shaped ball, strongly depends on magnetic parameters and properties of the particles. In brief, we have demonstrated, for the first time, impact on SLP of the accumulation of ellipsoid-shaped superparamagnetic nanoparticles into a sphere-shaped ball. This finding has essential suggestions for developing links between heating properties with loose aggregate and dense aggregate scenarios in the superparamagnetic condition.

Research Highlights

- A theoretical model has been developed to enhance the heating efficiency, which could be utilized in thermal therapies and calculated parameter dependence for superparamagnetic MNPs (approximative ellipsoid-shaped) within a sphere-shaped ball.
- When particles are closer together (less volume gap of a sphere-shaped ball), high SLP is found for the same number of particles.
- The influence of a number of particles in a sphere-shaped ball demonstrates that SLP of magnetic particles increases with the increasing number of particles (N), and after $N = 10$ particles, the SLP increment is insignificant.
- Frequency dependency on SLP of ellipsoid-shaped superparamagnetic nanoparticles is negligible when the frequency is higher than 10 kHz.

Received 17 December 2019, Accepted 31 January 2020, Scheduled 9 March 2020

* Corresponding author: Malka N. Halgamuge (malka.nisha@unimelb.edu.au).

¹ Department of Electrical and Electronic Engineering, The University of Melbourne, Parkville, VIC 3010, Australia. ² Beijing Key Laboratory of Bioelectromagnetism, Institute of Electrical Engineering, Chinese Academy of Sciences, Beijing, China. ³ University of Chinese Academy of Sciences, Beijing 100049, China.

- The Kneedle Algorithm was utilized to estimate the optimal parameter values, which is established on points of maximum curvature in a given data set (curve).
- In general, hence, it seems that the SLP of MNPs in a sphere-shaped ball also strongly depends on the magnetic parameters and properties of the particles.
- Developing links between heating properties with loose aggregate and dense aggregate scenarios in the superparamagnetic condition are essential.

1. INTRODUCTION

Magnetic nanoparticles (MNP) heating systems had numerous biomedical applications, including potential use in hyperthermia treatments such as cancer therapy and wound healing and arose as an efficient approach. Hyperthermia treatment relies on the certainty of the nanoparticle absorbs energy after absorbing an alternating magnetic field (AMF). Hence, the MNP acts as initiators of the converting energy from an AMF that could use in hyperthermia treatments.

Taking into account that superparamagnetism has dominated the literature of nanoparticle hyperthermia, it is beneficial to start computing the generated heat. Besides, views of “superparamagnetic” performance in hyperthermia have not been completely investigated [1]. The most of superparamagnetic nanoparticles are artificially synthesized. Superparamagnetism is an extraordinary feature of the single-domain magnets; however, not all single-domain magnets are essentially superparamagnetic [1].

The transformation of electromagnetic energy into heat using nanoparticles has been investigated in a considerable amount of literature [1–9] to be used in applications such as drug release and disease treatment, including cancer therapies. Nonetheless, less efficiency for this transformation led to obstruction utilizing this technology from a practical point of view. Hence, questions remain answered investigating particles with more significant heating properties and efficient transformation of electromagnetic energy into heat using nanoparticles.

The main aim of the present study is to gain more in-depth insight into the heat generation mechanisms of MNP and to interpret the particle properties, high-frequency electromagnetic field parameters, and possible optimization for future purpose in reliable hyperthermia treatments. The secondary aim is to explain the usability of the magnetic particles in a sphere-shaped ball, more efficiently. We developed theoretical strategies to enhance the heating efficiency, which could be utilized in thermal therapies and calculated parameter dependence for sphere-shaped ball consisting of superparamagnetic nanoparticles.

The remainder of this paper is as follows. In Section 2, we describe the specific loss power (SLP) in superparamagnetic nanoparticles. The dependency of features of the nanoparticles (such as mean particle size, number of particles, frequency and amplitude of the exposed field relaxation time, and volume gap between particles and a sphere-shaped ball) on the SLP or the heating effect in superparamagnetic MNPs was investigated. SLP for an individual magnetic particle (CASE A) and SLP for a sphere-shaped ball with N magnetic particles (CASE B) are calculated in Section 3 and Section 4. Additionally, the optimal parameter values are computed using Kneedle Algorithm to identify the accurate heating efficiency in Section 5, and in Section 6 we discuss the results. Section 7 explains the discussion, and Section 8 concludes the paper.

2. SPECIFIC LOSS POWER OF SUPERPARAMAGNETIC NANOPARTICLES

The heat generation mechanism in MNP can be associated with relaxation loss, which is in two types: Neel (or hysteresis loss) and Brownian relaxations. The relative influence of each method highly relies on shape, size, and the anisotropy of nanoparticles. The internal (Neel) and external (Brownian) sources of friction that drive a phase lag between the used magnetic field and the orientation of the magnetic moments manage to generate thermal losses. Using linear response models, with known Neel and Brownian relaxation times, SLP values for MNPs can be easily predicted [2].

The SLP or the heating effect in superparamagnetic nanoparticles depends remarkably on the magnetic properties of the particles that may change depending on their mean particle size, frequency and amplitude of the exposed signal as well as the width of the size distribution [3].

We developed theoretical strategies to enhance the heating efficiency, which could be utilized in thermal therapies and calculated parameter dependence for ellipsoid-shaped superparamagnetic nanoparticles.

2.1. Hydrodynamic Volume

The magnetic anisotropy and MNP core size affect the Neel relaxation time, while environmental influences, for example, the viscosity of the solvent, temperature, and MNP clusters size (hydrodynamic size) affect the Brownian relaxation time [12]. Hence, here, we calculate the hydrodynamic volume of MNP particles. Hydrodynamic volume for a particle with ellipsoid-shaped superparamagnetic nanoparticles is given by

$$V_H = \frac{4\pi(a + \delta)(b + \delta)^2}{3} \quad (1)$$

where δ is the thickness of a surfactant layer of the particle, and $2a$, $2b$, $2b$ are particle axes as shown in Figure 1.

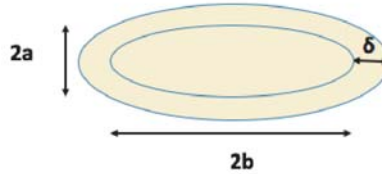


Figure 1. Magnetic particle with lengths $2a$, $2b$, $2b$ axis, and δ thickness.

2.2. Shape Factor

The magnetic property of the magnetic particle is related to its shape factor, and it is given as the ratio between the length and width of the particle. It is provided by

$$Sf = \frac{Length}{Width} = \frac{2b}{2a} = \frac{b}{a}. \quad (2)$$

The shape factor of the ellipsoid shape MNPs can be approximately 1.424, as given in [10].

2.3. Neel and Brownian Relaxation Time

In superparamagnetic particles, the total sum of heat generation depends on the relaxation methods (Neel losses and Brownian losses). Thermal relaxation in direct response theory by estimating a relaxation time constant (τ) is invented by two distinct thermal relaxation mechanisms: Brownian relaxation (τ_B) in which the nano-particle and magnetic moment rotate concurrently, and Neel relaxation (τ_N) in which the magnetic moment rotates with respect to the crystal.

With reducing particle size, the energy limit for magnetization reversal drops, and as a consequence, thermal fluctuations lead to relaxation phenomena [13]. Hence, quasi-statically measured hysteresis loops are narrow, and determined SLP becomes less than data measured direct by calorimetry. This phenomenon, so-called Neel relaxation [13] due to the variation of the magnetic moment direction, crossed an anisotropy barrier. The characteristic relaxation time from a nanoparticle, τ_N , is provided by the ratio of the anisotropy energy ($K_u V$) to the thermal energy ($k_B T$) as

$$\tau_N = \tau_0 \exp(\Gamma)$$

where $\Gamma = K_u V_M / k_B T$, τ_0 is the constant 10^{-9} sec, K_u the magnetic anisotropy energy density, V_M the particle volume, k_B the Boltzmann's constant, and T the temperature.

When the angle between the magnetization and applied magnetic field is given by γ as shown in [1], the Neel relaxation time is given by

$$\tau_N = \frac{\sqrt{\pi}}{2} \tau_0 \frac{\exp(\Gamma')}{\sqrt{\Gamma'}} \quad (3)$$

where $\Gamma' = (K_u V_M - HM \cos \gamma)/k_B T$.

The second relaxation mechanism happens due to the reorientation of the entire particle if the particle is freely mobile inside a suspension medium of viscosity η . This mechanism is so-called Brown relaxation with the characteristic relaxation time given by [14]

$$\tau_B = 3\eta V_H / k_B T \quad (4)$$

where η is the viscosity coefficient of the medium, k_B the Boltzmann's constant (1.38×10^{-23}), T the absolute temperature (K), and V_H is considered as the hydrodynamic volume of the particle that is greater than the magnetic volume for particle radius R . Hence $V_H = 4\pi(a + \delta)(b + \delta)^2/3$ where δ is the thickness of a surfactant layer of the particle. The Brown mechanism creates the production of heat due to the viscous friction between the rotating particle and surrounding medium.

In super-paramagnetic MNPs, both Brownian and Neel relaxation processes occur, simultaneously. Hence, the effective relaxation time which is related to the heat dissipation of MNPs, τ_r , is given by using Eqs. (3) and (4) $\tau_r = \tau_N \tau_B / (\tau_N + \tau_B)$.

2.4. Heat Generation Based on Neel and Brownian Relaxation Time

The frequency dependency of the relaxation of the particle method is well examined experimentally. This is done by including spectra of the complex susceptibility. The imaginary part $\chi''(f)$ that is related to magnetic losses is given by [15]

$$\chi''(f) = \chi_0 \phi / (1 + \phi^2).$$

Here $\phi = \omega \tau_r$ and $\chi_0 = \mu_0 M_s^2 V_M / (\alpha k_B T)$, where M_s is the saturation magnetization. and α is the constant value between 1 and 3. The heating efficiency of different MNPs can be explained as their SLP, or the loss power density, or power dissipation P within the valid range of linear response approach. This is given by [16] $P = \mu_0 \pi \chi''(f) H^2 f$. It can be further simplified as

$$P = \frac{\pi \mu_0^2 f H^2 M_s^2 V_M \phi}{\alpha k_B T (1 + \phi^2)}. \quad (5)$$

The most vital property for magnetic hyperthermia treatments is the SLP which describes that the energy is dissipated into heat once the particle magnetic moments are subject to the external magnetic field.

3. CASE A — SLP FOR INDIVIDUAL MAGNETIC PARTICLE

Consider individual (single) magnetic particle with ellipsoid-shape, as shown in Figure 2. Using Equation (1), the hydrodynamic volume for one magnetic particle, V_{H_1} , is given as

$$V_{H_1} = \frac{4\pi(a_1 + \delta_1)(b_1 + \delta_1)^2}{3} \quad (6)$$

where δ_1 is the thickness of a surfactant layer of the particle, and $2a_1$ and $2b_1$ are the width and length of a magnetic particle. Using Equation (2), the shape factor for one magnetic particle is given by

$$Sf_1 = \frac{2b_1}{2a_1} = \frac{b_1}{a_1}.$$

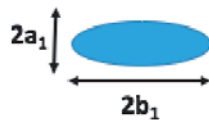


Figure 2. Case A (SLP for Individual Magnetic Particle) - Magnetic particle with ellipsoid-shaped ($2a_1$, $2b_1$, $2b_1$ axis).

The Neel relaxation (τ_{N_1}) and Brown relaxation (τ_{B_1}) with the characteristic relaxation time for one particle can be determined using Equations (3) and (4), and are given by $\tau_{B_1} = 3\eta V_{M_1}/k_B T$ and $\tau_{N_1} = \sqrt{\pi}\tau_0 \exp(\Gamma')/(2\sqrt{\Gamma'})$ where $\Gamma' = (K_u V_{M_1} - HM \cos \gamma)/k_B T$.

Now we can apply this to the magnetic particle with ellipsoid-shape, where $SLP = P/\rho$, where ρ is the density of magnetic materials. Hence, using Equations (5) and (6), SLP of the magnetic particle with ellipsoid-shape, SLP_1 , can be calculated as

$$SLP_1 = \frac{2\pi^2 \mu_0^2 f^2 H^2 M_s^2 V_{M_1} \tau_{r_1}}{\alpha k_B T [1 + (2\pi f \tau_{r_1})^2] \rho}.$$

However, since the volume of the ellipsoid-shaped magnetic particle is $V_{M_1} = 4\pi a_1 b_1^2/3$, as shown in Figure 2, SLP_1 can be rewritten as

$$SLP_1 = \frac{8\pi^3 \mu_0^2 f^2 H^2 M_s^2 a_1 b_1^2 \tau_{r_1}}{3\alpha k_B T [1 + (2\pi f \tau_{r_1})^2] \rho} \quad (7)$$

where $\tau_{r_1} = \tau_{N_1} \tau_{B_1} / (\tau_{N_1} + \tau_{B_1})$.

4. CASE B: SLP FOR A SPHERE-SHAPED BALL WITH N MAGNETIC PARTICLES

The magnetic particle hyperthermia has demonstrated effectiveness in clinical trials, which have shown the potential of magnetic hyperthermia for cancer and proved that patients could take this therapy without inconvenience or extreme side reactions [7]. The superparamagnetic nanoparticles are easy to aggregate to form a sphere. Most of the artificially synthesized magnetic particles (100 nm–10 μ m) are composed of superparamagnetic nanoparticles [1]. In this section, we develop theoretical strategies to enhance the heating efficiency, which could be utilized in thermal therapies and calculated parameter dependence for superparamagnetic MNPs (approximative ellipsoid-shaped), within a sphere-shaped ball.

Consider a sphere-shaped ball with N number of magnetic particles, as shown in Figure 3.

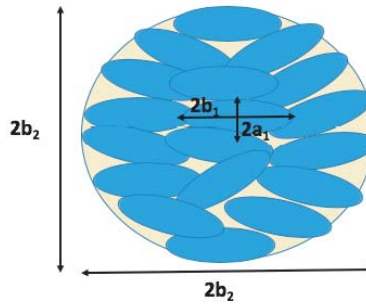


Figure 3. Case B (SLP for a Sphere-shaped Ball with N Magnetic Particles): Specific loss power of magnetic particles in a sphere-shaped ball or magnetic sphere (volume, $V_{M_2} = 4\pi b_2^3/3$) with N magnetic particles ($2a_1, 2b_1, 2b_1$ axis) where V_{gap} is volume gap between a sphere and N magnetic particles.

4.1. Volume Gap (V_{gap}) for CASE B

Consider a sphere with N magnetic particles. The magnetic volume of the sphere is $V_{M_2} = 4\pi b_2^3/3$ and N magnetic particles with $2a_1, 2b_1, 2b_1$ axes. Here we define that the volume gap (V_{gap}) is the volume between the sphere and N magnetic particles (Figure 3).

$$V_{gap} = N \frac{4\pi a_1 b_1^2}{3} \beta, \quad (8)$$

where we assume that β is about 20%–30%. Using Eq. (8),

$$V_{M_2} = \frac{4\pi b_2^3}{3} = N \frac{4\pi a_1 b_1^2}{3} + V_{gap}. \quad (9)$$

Using Eqs. (8) and (9),

$$b_2^3 = (4\pi N a_1 b_1^2 + 3V_{gap})/4\pi. \quad (10)$$

4.2. Hydrodynamic Volume for CASE B

Using Equation (1), the hydrodynamic volume for a sphere-shaped ball with N magnetic particles, V_{H_2} , is given by

$$V_{H_2} = \frac{4\pi \left[\left(N a_1 b_1^2 + \frac{3V_{gap}}{4\pi} \right)^{\frac{1}{3}} + \delta_2 \right]^3}{3} \quad (11)$$

where δ_2 is the thickness of a surfactant layer of the volume of N particles.

Neel relaxation time is insensitive to the geometric shape, and instead, it relies on the anisotropy of the material concerned. A sphere is a special case of an ellipsoid, hence, the formula for ellipsoids could be used for a sphere. In this study, we use the same Neel relaxation time formula for spherical particles. Here we assume that there is no relative motion (rotation) among the superparamagnetic nanoparticles in the sphere. The Neel relaxation (τ_{N_1}) and Brown relaxation (τ_{B_1}) with the characteristic relaxation time for N particles can be determined using Equations (3) and (4), and are given by $\tau_{B_2} = 3\eta V_{H_2}/k_B T$ and $\tau_{N_2} = \sqrt{\pi}\tau_0 \exp(\Gamma')/(2\sqrt{\Gamma'})$ where $\Gamma' = (K_u V_{M_2} - HM \cos \gamma)/k_B T$. Now we can apply this to a

Table 1. Parameters of SLP calculation of magnetic particles.

Symbol	Parameter	Values
f	Frequency of the AC magnetic field	80 kHz
ρ	Density of the magnetic materials	5240 kg/m ³ [7]
μ	Permittivity = $\mu_r \times \mu_0$	$4\pi \times 10^{-7}$
M_S	Saturation magnetisation	480 kA/m [7]
H	Field strength/amplitude of the AC magnetic field	6.9 kA/m
Sf_1	Shape factor for the magnetic particle	$b_1/a_1 = 1.424$ [10]
$2b_1$	Length/Diameter of the magnetic particle	10 nm (6–12) nm
$2a_1$	Width of the magnetic particle	$2b_1/Sf_1$ nm
$2b_2$	Width of a sphere-shaped ball with N particles	Eq. (10)
β	Volume gap percentage between a sphere and particles	20–30%
N	Number of magnetic particles	60
T	Absolute temperature	293 K
V_{M_1}	Magnetic volume for individual (single) magnetic particle	$4\pi a_1 b_1^2/3$
V_{M_2}	Magnetic volume for a sphere-shaped ball with N particles	$4\pi b_2^3/3$ or Eq. (9)
V_{gap}	Volume gap between a sphere and N magnetic particles	Eq. (8)
V_{H_1}	hydrodynamic volume for one magnetic particle	Eq. (6)
V_{H_2}	hydrodynamic volume for a sphere-shaped ball with N particles	Eq. (11)
δ_1	Thickness of a surfactant layer for one magnetic particle	2 nm [2]
δ_2	Thickness of a surfactant layer for a sphere-shaped ball with N particles	3 nm
K_u	Magnetic anisotropy constant of the particles	32000 J/m ³ [6]
k_B	Boltzman's constant for particle	1.38×10^{-23} J/K [11]
τ_0	Average relaxation time due to thermal fluctuation	10^{-9} s [4]
τ_B	Brownian relaxation time constant	-
τ_N	Neel relaxation time constant	-
α	Constant	3 ($\approx 1-3$)
η	Viscosity of medium	1×10^{-3} Pa s [5]
γ	Angle between the applied magnetic field and magnetisation	$1 - \pi$

sphere-shaped ball with ellipsoid-shaped magnetic particles, where $SLP = P/\rho$. It should be noticed that ρ is the density of the ball (not the particles). The densities are the difference between particles and balls, especially when the gap is enlarged. Hence, using Equation (5) and (11), SLP of a sphere-shaped ball with N particles, SLP_2 can be calculated as

$$SLP_2 = \frac{2\pi^2\mu_0^2f^2H^2M_s^2V_{M_2}\tau_{r_2}}{\alpha k_B T [1 + (2\pi f\tau_{r_2})^2]\rho}$$

where $\tau_{r_2} = 4\pi\eta(a_2 + \delta_2)^2(b_2 + \delta_2)/k_B T$. The magnetic volume of a sphere-shaped ball with N particles can be calculated as $V_{M_2} = 4\pi a_2^2 b_2/3 = 4\pi a_1 b_1^2 N/3$, as shown in Figure 3. Hence, SLP_2 can be rewritten as

$$SLP_2 = \frac{8\pi^3\mu_0^2f^2H^2M_s^2a_1b_1^2N\tau_{r_2}}{3\alpha k_B T [1 + (2\pi f\tau_{r_2})^2]\rho} \quad (12)$$

where $\tau_{r_2} = \tau_{N_2}\tau_{B_2}/(\tau_{N_2} + \tau_{B_2})$.

5. OPTIMIZATION TECHNIQUE

We use the Kneedle Algorithm to obtain the optimal point, which is established on points of maximum curvature in a given data set (curve). The knees are nearly the set of points in a curve that are local maxima which illustrate valuable points that system designers have selected to best balance inherent tradeoffs [17].

The Kneedle Algorithm is based on the idea that the points of maximum curvature in a data set, or the knees, are approximately the set of points in a curve that is local maxima. Let D_b be the finite set of x_{b_i} and y_{b_i} values which defines the smooth curve. Next, we consider that D_{bn} represents the set of differences between the x - and y -values. The threshold value is given by T_{imax} .

Algorithm 1 Optimal Point Calculation

Load coordinates of all the points of the curve

$$D_b = (x_{b_i}, y_{b_i}) \in \mathbb{R} \mid x_{b_i}, y_{b_i} \geq 0$$

Get the first point

Get vector between first and last point

Normalize the line vector

$$D_{bn} = \{x_{bn_i}, y_{bn_i}\}, \text{ where}$$

$$x_{bn_i} = (x_{b_i} - \min\{x_b\})/(\max\{x_b\} - \min\{x_b\}),$$

$$y_{bn_i} = (y_{b_i} - \min\{y_b\})/(\max\{y_b\} - \min\{y_b\}).$$

Calculate the distance (D_d) from each point to the line

$$D_d = \{x_{d_i}, y_{d_i}\}, \text{ where}$$

$$x_{d_i} = x_{bn_i},$$

$$y_{d_i} = y_{bn_i} - x_{bn_i}.$$

Calculate local maximum (D_{imax}) points

$$D_{imax} = \{x_{imax}, y_{imax}\}, \text{ where}$$

$$x_{imax} = x_{d_i},$$

$$y_{imax} = y_{d_i} \mid y_{d_{i-1}} < y_{d_i}, y_{d_{i+1}} < y_{d_i}.$$

Calculate local maximum (D_{imax}) points

$$T_{imax} = y_{imax} - S \frac{\sum_{i=1}^{n-1} (x_{bn_{i-1}} - x_{bn_i})}{n-1}.$$

Find the local maximum

$$(x_{d_j}, y_{d_j}), \text{ where } j > i,$$

$$y = T_{imax}, \forall (x_{imax}, y_{imax}),$$

$$x = x_{imax}.$$

In this study, we assume that maghemite nanoparticle (MNP) consists of maghemite (Fe_3O_4), and parameters are given in Table 1. This calculation is valid for superparamagnetic nanoparticles. The optimal values for each parameter at the ‘‘knee’’ point is observed.

6. RESULTS

Observing the optimal parameters for magnetic nanoparticle-based hyperthermia for different diseases treatment in biomedical applications such as cancer and wound healing is crucial. We developed theoretical strategies to enhance the heating efficiency that could be utilized in thermal therapies and calculate parameter dependence for superparamagnetic MNPs. Many studies show that there are factors which may impact the heating efficiency of magnetic nanoparticles, including both physical and magnetic properties of the particles and the frequency and magnitude of the applied magnetic field. In this analysis, properties of several types of relevant magnetite parameters, especially, (i) frequency and amplitude of the AC magnetic field, (ii) particle diameter, (iii) a number of particles, (iii) relaxation time, and (iv) volume gap between particles and a sphere-shaped ball are investigated concerning optimizing thermal therapies for hyperthermia.

6.1. Case A — SLP for Individual Magnetic Particle

We use SLP model as shown in Equation (7) to compare SLP for magnetic with one particle introduced in Section 3. Dependence of various magnetic parameters and relaxation mechanism on the SLP of one magnetic particle are observed. For this analysis, we consider: frequency = 300 kHz, field amplitude = 14 kA/m, $Sf_1 = 1.424$, $2b_1 = 10$ nm, and $a_1 = b_1/Sf_1$, unless different values are mentioned in the subfigures. Other parameters are shown in Table 1. Magnetic relaxation loss is one of the heating techniques of MNPs. The relationship between Neel relaxation time (τ_N) and Brownian relaxation time (τ_B) is related to the particle diameter. The Brown relaxation is well studied while Neel relaxation is limited to the relatively small magnetic particle size. When the particle diameter is less than 20 nm, τ_N cannot be ignored. Hence, in this analysis, both τ_N and τ_B were observed.

The Brownian relaxation time of fluids is associated with the hydrodynamic particle volume V_h according to the Equation (4). It is observed that SLP increases with increasing the length of the magnetic particle between $1 < 2b_1 < 12$ nm, as shown in Figure 4(a). When the particle length is greater than 5 nm, the significant increment of SLP is found. Dependence of particle diameter of the magnetic particle ($2b_1$) on SLP with optimal parameters is shown in Figure 5. Based on optimum parameter settings for each applied field strength or amplitude of the AC magnetic field can be obtained from the

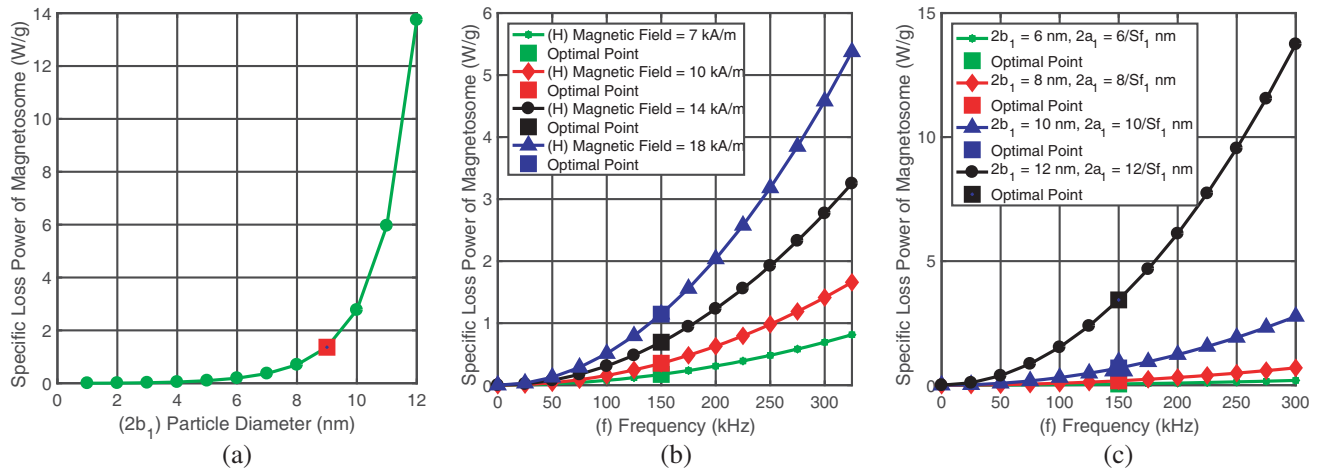


Figure 4. CASE A (SLP for Individual Magnetic Particle): Dependence of the particle diameter ($2b_1$), the frequency of the AC magnetic field (f) on SLP with optimal parameters. For this analysis, we consider: frequency = 300 kHz, field amplitude = 14 kA/m, $Sf_1 = 1.424$, $2b_1 = 10$ nm and $a_1 = b_1/Sf_1$, unless different values are mentioned in the subfigures. Other parameters are shown in Table 1. (a) Dependence of particle diameter of the magnetic particle ($2b_1$) on SLP. (b) Dependence of the frequency of the AC magnetic field (f) on SLP for different amplitude (H). (c) Dependence of the frequency of the AC magnetic field (f) and shape factor ($S_f = 2b_1/2a_1$) on the SLP.

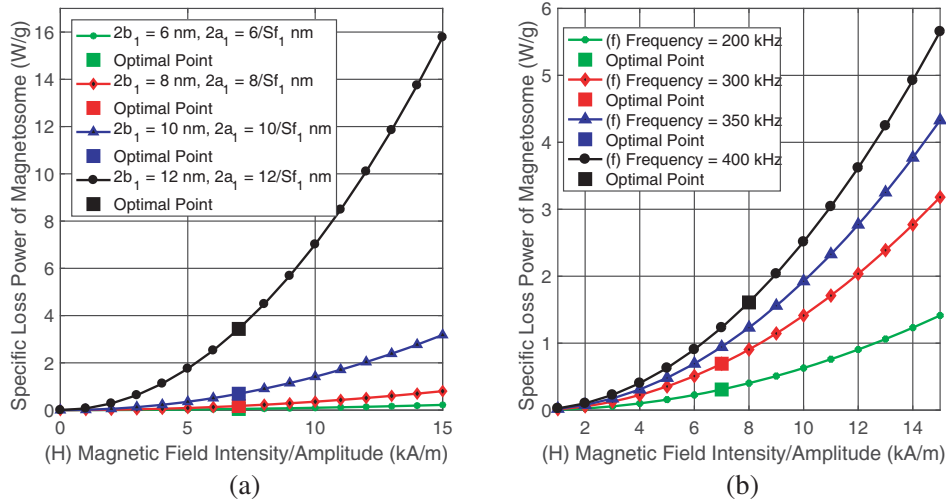


Figure 5. CASE A (SLP for Individual Magnetic Particle): Dependence of amplitude (H), frequency (f) of the AC magnetic field and shape factor ($S_f = 2b_1/2a_1$) on SLP with optimal parameters. For this analysis, we consider: frequency = 300 kHz, field amplitude = 14 kA/m, $Sf_1 = 1.424$, $2b_1 = 10$ nm and $a_1 = b_1/Sf_1$, unless different values are mentioned in the subfigures. Other parameters are shown in Table 1. (a) Dependence of amplitude (H) of the AC magnetic field and shape factor ($S_f = 2b_1/2a_1$) on SLP. (b) Dependence of amplitude (H) of the AC magnetic field and frequency (f) on SLP.

“knee” point of the corresponding curves. Finding optimal frequency for the better SLP is important in MNP hyperthermia. Hence, Figure 4(b) shows the dependence of applied frequency (f) on SLP for the different applied field strengths (H). This demonstrates the direct impact of the applied field strength between $1 < H < 18$ kA/m on SLP for the same length of the magnetic particle ($2b_1 = 10$ nm). The frequency versus SLP curve for different fields suggests that operating at higher fields rather than higher frequencies would be more effective for hyperthermia. This was also observed in previous research by Muller et al. (2013) [18]. By keeping the same applied field strength (14 kA/m), we varied the length of the magnetic particle ($6 < 2b_1 < 12$ nm) to observe the changes on SLP. The significant increment of SLP was found when increasing the particle length. The magnetic property of the magnetic particle is also related to the frequency on the SLP. Both these concepts are observed in Figure 4(c).

Similarly, Figure 5(a) shows the dependence of the amplitude of the AC magnetic field and the length of the magnetic particle on the SLP where the frequency of the applied field is constant ($f = 300$ kHz). Then we varied the amplitude of the AC magnetic field ($0 < H < 18$ kA/m) and the frequency ($200 < f < 400$ kHz) to observe the impact on SLP for the same length of the magnetic particle ($2b_1 = 10$ nm) as shown in Figure 5(b). The significant increment was found on SLP.

Recent studies have observed the lack of agreement among experimental studies of concentration effects on SLP; nonetheless, much of the confusion comes from the varying effect of relaxation time on SLP in Brownian versus Neel-dominated systems [8]. Moreover, the application of the relaxation principle to hyperthermia concerns the dependence of field amplitude on SLP.

Our measurements (Table 4) showed that optimal positions of SLP for one magnetic particle (CASE A) could be adjusted by varying field strength (H) and frequency (f). Generally, SLP of the magnetic particle increases with an increase of the exposed H and f ; however, using the Algorithm 1 optimal values (“knee” points) were obtained (set of points in a curve that is local maxima) as shown in Table 4. The Kneedle Algorithm would be invaluable to understand how to regulate the thermal therapies necessitating magnetic hyperthermia treatments.

Further study should be carried out on the dependence of different magnetic parameters and relaxation mechanism on SLP when considering a sphere-shaped ball with N magnetic particles instead of one magnetic particle. We examine this further in the next section.

Table 2 outlines some published (estimated) values on magnetic heating of small nanoparticles with a width less than or equal to 12 nm.

Table 2. Published specific loss power (SLP) measurements (CASE A) for several magnetic particles (diameter d , magnetic field strength H and frequency f).

Study	Material	(f) Frequency (kHz)	(H) Field (kA/m)	(d) Diameter (nm)	SLP (W/g)
Fantechi et al. (2015) [19]	Fe_3O_4	183	12	8	6.5
Fantechi et al. (2014)	Ferritin with Fe_2O_4	183	12.4	6	<0.01
This Study (2019)	Fe_3O_4	300	14	6	0.191
This Study (2019)	Fe_3O_4	300	14	8	0.698
This Study (2019)	Fe_3O_4	300	14	10	2.77
This Study (2019)	Fe_3O_4	300	14	12	13.74

6.2. Case B: SLP for a Sphere-Shaped Ball with N Magnetic Particles

We use Equation (12) to compare SLP for magnetic particles with N particles introduced in Section 4. Interesting correlation between particle diameter and SLP is observed in superparamagnetic particles in a sphere-shaped ball, where the SLP increases with increasing magnetic particle diameter up to $2\text{ nm} < 2b_1 < 4\text{ nm}$. When the diameter is $2b_1 > 5\text{ nm}$, the slight increment is observed. From Figure 8(c), it can be noticed that magnetic particles yield the most substantial heating rates with the particle diameter size range of 4–5 nm.

It is beneficial to manage the temperature improvement needed for a unique application with as low as possible amount of MNP. Hence, the SLP of the MNP that is measured in watts per gram of magnetic material to be utilized must be large enough. This is especially critical for applications when target concentration is very low, for example, in the antibody targeting of tumors [4]. Hence, we further observed the impact of a number of particles on SLP (Figures 6(a) and (b)) to verify this

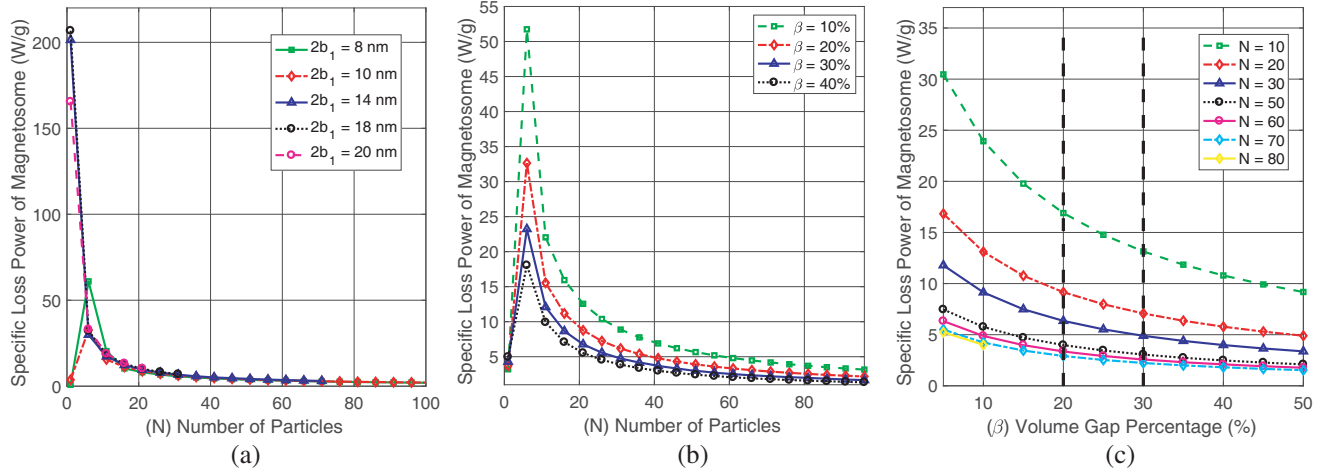


Figure 6. CASE B (SLP for a Sphere-shaped Ball with N Magnetic Particles): Dependence of a number of particles (N), particle diameter ($2b_1$) and volume gap percentage (β) on SLP with optimal parameters. For this analysis, we consider: frequency = 300 kHz, field amplitude = 14 kA/m, $Sf_1 = 1.424$, $2b_1 = 10\text{ nm}$ and $a_1 = b_1/Sf_1$, unless different values are mentioned in the subfigures. Other parameters are shown in Table 1. (a) Dependence of a number of particles (N) and particle diameter ($2b_1$) on SLP. (b) Dependence of a number of particles (N) and volume gap percentage (β) on SLP. It should be noticed that the density of the ball is changed with the gap. (c) Dependence of volume gap percentage (β) between a sphere and particles (β) and a number of particles (N) on SLP.

Table 3. Dependence of a number of particles (N) and volume gap percentage (β) on SLP.

No of Particles	SLP when $\beta = 40\%$	SLP when $\beta = 30\%$	SLP when $\beta = 20\%$	SLP when $\beta = 10\%$
6	18.06	23.22	32.64	51.74
11	9.91	12.08	15.55	22.04
16	7.08	8.65	11.17	15.94
21	5.53	6.77	8.76	12.55
26	4.54	5.57	7.23	10.39
31	3.86	4.74	6.16	8.87
36	3.36	4.13	5.38	7.75
41	2.98	3.67	4.77	6.89
46	2.68	3.30	4.29	6.21
51	2.43	2.99	3.90	5.65
56	2.23	2.74	3.58	5.19
61	2.06	2.53	3.31	4.80

and found a consistent trend. When particles were close together (less volume gap of a sphere-shaped ball or less percentage of β), high SLP was observed for the same number of particles as shown in Table 3. Figure 6(a) shows the SLP increases with an increasing particle diameter when the number of particles (N) is less than 10, and after this point, SLP decreases with a number of particles (N), and no significant differences on SLP are found.

We also observe that SLP decreases with an increasing β (volume gap percentage between the sphere and particles). For all β values, the highest SLP was observed when a number of particles $N = 6$. It should be noticed that the density of the ball is changed with the gap. There is a volume gap between a sphere-shaped ball and superparamagnetic particles which relies upon the particle number. We modelled the relationship (see Appendix, Figure 10) among a number of particles, sphere volume, and volume gap for a different particle diameter ($2b_1 = 6, 8, 10, 12$ nm). Consequently, for this study, we use the volume gap as 20-30% of the total volume of a sphere-shaped ball; however, we observed the impact on the variation of the volume gap to SLP. Dependence on volume gap percentage between the sphere and particles (β) shows (Figure 6(c)) the decrement of SLP with the increment of β ; however, SLP increases with the number of particles (N).

These findings further support the idea of dipolar interaction between nanoparticles. Due to the increment of the mean distance between magnetic nanoparticles, the dipolar interaction energy between nanoparticles will be decreased. Eventually, particles could decrease their capability to heat their neighboring medium. Another thinking for this relationship could be the demagnetization field [20]. It is undoubtedly induced inside total magnetization, as it reduces the local magnetic field exposure (direct) for all particles, which leads, hence, to a reduction of the SLP.

Owing to their small particle sizes due to superparamagnetic behavior, for this study, we observed the particle diameters $2b_1 = 6, 8, 10, 12$ nm. Particle size dependence of the magnetic hyperthermia properties of superparamagnetic nanoparticles was observed with varying frequency. The dependence of the frequency (f) of the AC magnetic field and particle diameter ($2b_1$) on SLP were observed, as shown in Figure 7(a), the direct impact of particle diameter ($2b_1$) and frequency on SLP. The optimal point for frequency versus SLP depends on the particle diameter. These optimal values are shown in Table 4. The more surprising correlation is with the particle diameter and frequency of the AC magnetic field on SLP. We observe that SLP does not vary when frequency is higher than 51 kHz for $2b_1 = 12$ nm particles, 80 kHz for $2b_1 = 10$ nm particles, 90 kHz for $2b_1 = 8$ nm particles, and 121 kHz for $2b_1 = 6$ nm particles (Figure 7(b)). Further analysis shows the frequency (f) dependence of SLP for different applied field amplitudes (H) (Figure 7(c)). This demonstrates the direct impact of the applied field amplitude $7 < H < 18$ kA/m on SLP; however, SLP does not vary when applied frequency is higher than 4–20 kHz.

Further, we observe the dependence of the SLP with the amplitude of the applied AC field for different frequencies. Figure 8(a) shows that the SLP increases with increasing amplitude of the AC

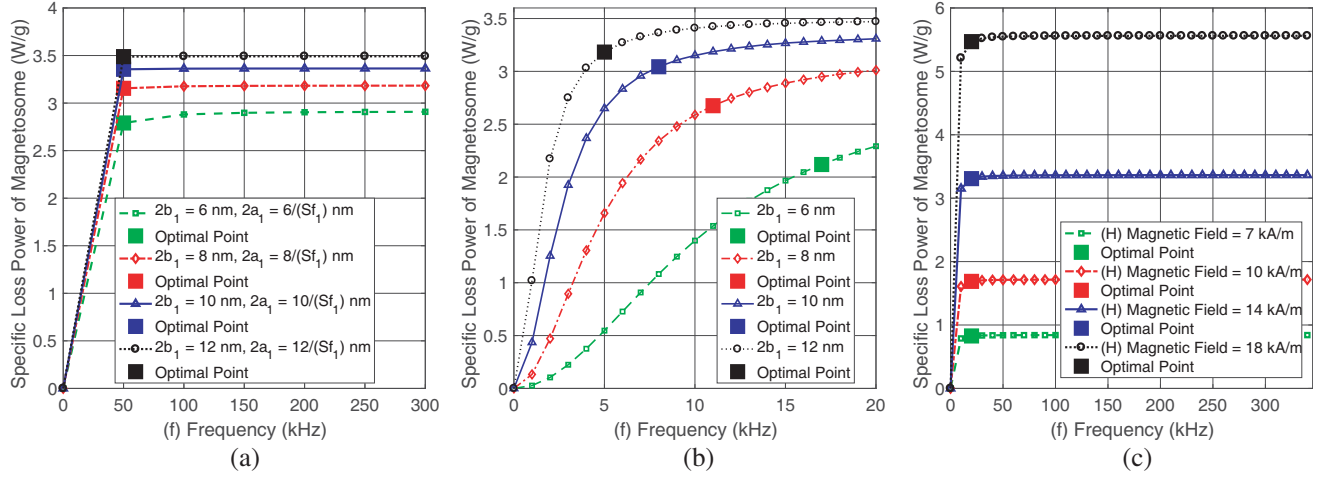


Figure 7. CASE B (SLP for a Sphere-shaped Ball with N Magnetic Particles): Dependence of the frequency (f) and the applied field amplitude (H) of the AC magnetic field, and particle diameter ($2b_1$) on SLP with optimal parameters. For this analysis, we consider: frequency = 300 kHz, field amplitude = 14 kA/m, $Sf_1 = 1.424$, $2b_1 = 10$ nm and $a_1 = b_1/Sf_1$, unless different values are mentioned in the subfigures. Other parameters are shown in Table 1. (a) Dependence of the frequency (f) of the AC magnetic field, and particle diameter ($2b_2$) on SLP. (b) Dependence of frequency (f) of the AC magnetic field and diameter of the magnetic nanoparticle ($2b_2$) on SLP. (c) Dependence of the applied field amplitude (H) and frequency (f) of the AC magnetic field on SLP.

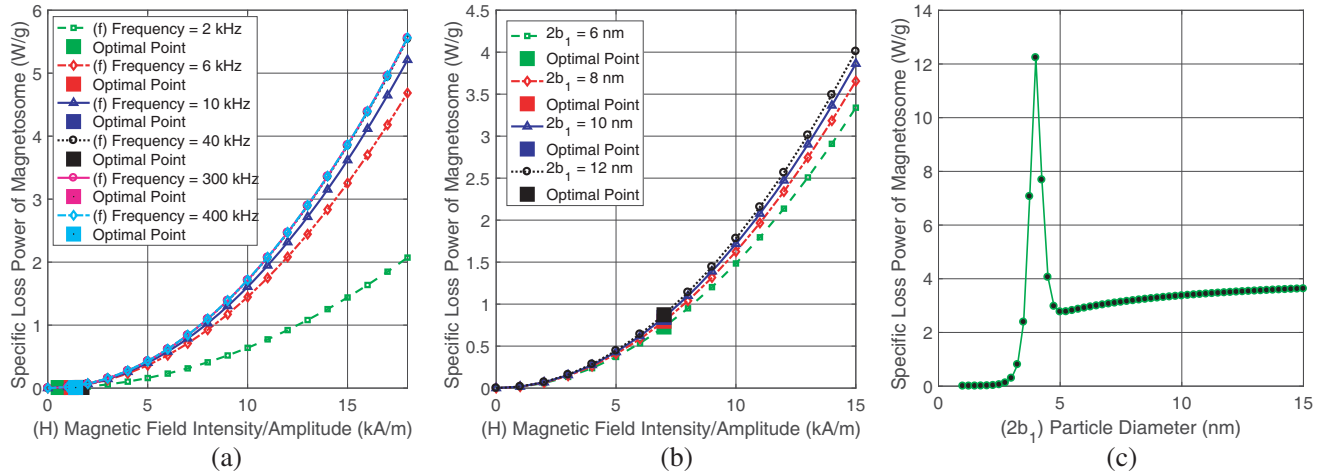


Figure 8. CASE B (SLP for a Sphere-shaped Ball with N Magnetic Particles): Dependence of the frequency (f), the applied field amplitude (H) of the AC magnetic field, and particle diameter ($2b_1$) on SLP with optimal parameters. For this analysis, we consider: frequency = 300 kHz, field amplitude = 14 kA/m, $Sf_1 = 1.424$, $2b_1 = 10$ nm and $a_1 = b_1/Sf_1$, unless different values are mentioned in the subfigures. Other parameters are shown in Table 1. (a) Dependence of the applied field amplitude (H) and frequency (f) of the AC magnetic field on SLP. (b) Dependence of the applied field amplitude (H) and particle diameter ($2b_1$) on SLP. (c) Dependence of diameter of the particle ($2b_1$) on SLP.

magnetic field (H). However, we find an insignificant impact on the frequency when it is greater than 10 kHz.

We further analyze this relationship for different particle diameters. Figure 8(b) shows the SLP increases with increasing amplitude of the AC magnetic field (H). However, we find an insignificant

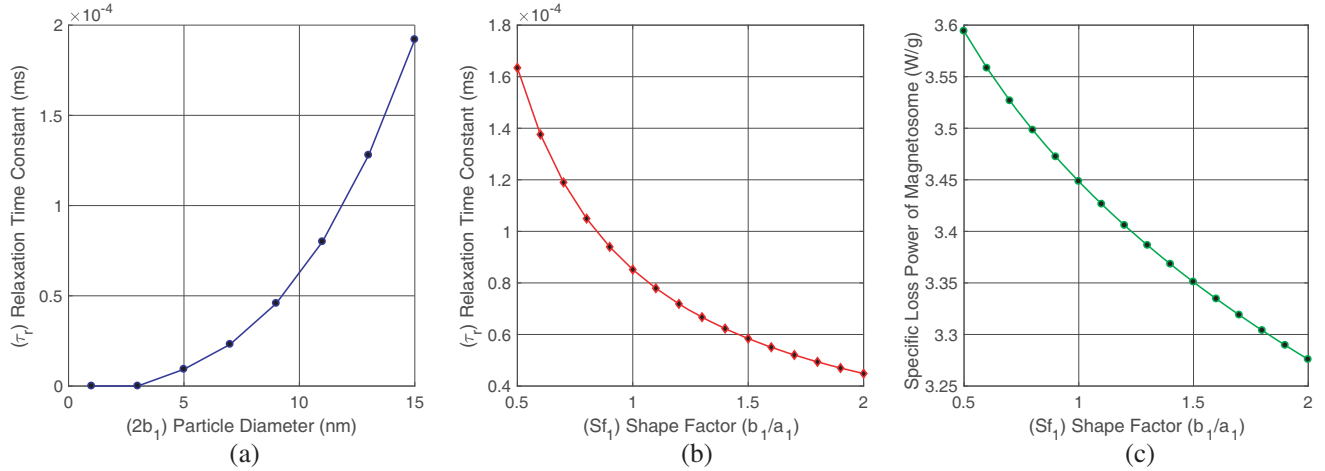


Figure 9. CASE B (SLP for a Sphere-shaped Ball with N Magnetic Particles): Dependence of diameter of the particle ($2b_1$), shape factor (Sf_1), and relaxation time (τ_r) on SLP with optimal parameters. For this analysis, we consider: frequency = 300 kHz, field amplitude = 14 kA/m, $Sf_1 = 1.424$, $2b_1 = 10$ nm and $a_1 = b_1/Sf_1$, unless different values are mentioned in the subfigures. Other parameters are shown in Table 1. (a) Dependence of diameter of the particle ($2b_1$) on relaxation time (τ_r). (b) Dependence of shape factor (Sf_1) on relaxation time (τ_r). (c) Dependence of shape factor (Sf_1) on SLP.

impact on the particle diameter ($2b_1$).

It is apparent in superparamagnetic particles that the aggregate sum of heat generation depends on the relaxation processes. The relaxation time (τ_r) (Neel losses and Brownian losses) increases with an increasing particle diameter, as shown in Figure 9(a). Relaxation processes that regulate the heating properties of superparamagnetic nanoparticles are further observed regarding the shape factor of the particle. The SLP decreases with an increasing shape factor ($Sf_1 = b_1/a_1$) of the magnetic particles which is observed in Figure 9(b). Dependence of shape factor (Sf_1) on the relaxation time (τ_B) is observed, and SLP decreases with an increasing shape factor of the nanoparticle.

Table 4 shows that optimal positions of SLP with N magnetic particles in a sphere-shaped ball (CASE B) can be adjusted by varying field strength (H), frequency (f), number of particles (N), and the volume gap between particles and a sphere-shaped ball. Usually, SLP of magnetic particles increases with an increase of the exposed H and f ; however, using the Algorithm 1 optimal values (“knee” points) are obtained as shown in Table 4. These knees typically represent important points that experimental designers could choose to accomplish the best stability in inherent tradeoffs between performance and usefulness. Besides this, future studies could explore the multivariable optimization technique by considering several variables.

7. DISCUSSION

Magnetic nanoparticle (MNP) serves as initiators of the converting energy from the AC magnetic field (AMF) into heat and arose as an efficient approach for biomedical applications using hyperthermia technique. This work utilizes well-known models in magnetic fluid science to estimate heating rate (SLP) in samples exposed to an alternating magnetic field. Superparamagnetic particles are identified to be efficient and steady transporters of thermoremanent magnetization.

There is a threshold of superparamagnetic particle size that suppresses the thermal activation, and from our results, it is noticed that the threshold is about 0–3 nm. In contrast, Neel’s (1999) findings [13] showed that for Fe_3O_4 [13] threshold was about 0–20 nm. Nonetheless, Neel’s (1999) investigation was not for the superparamagnetic particles. In contrast, Butler (1975) [21] showed that two-domain configuration is to be more applicable to fine-grained magnetite than to single-domain particles. The results of this study indicate that superparamagnetic particles produce the most substantial heating rates with the particle diameter size range of 4–5 nm. This finding seems consistent with Rosensweig et

Table 4. Optimal parameters for CASE A & B using Algorithm 1.

Figure No	Condition	Optimal Values (“Knee” Points)
CASE A (SLP for one magnetic particle)		
Fig. 5(a)	$H = 7 \text{ kA/m}$	$f = 150 \text{ kHz}$, SLP = 0.17 W/g
	$H = 10 \text{ kA/m}$	$f = 150 \text{ kHz}$, SLP = 0.35 W/g
	$H = 14 \text{ kA/m}$	$f = 150 \text{ kHz}$, SLP = 0.69 W/g
	$H = 18 \text{ kA/m}$	$f = 150 \text{ kHz}$, SLP = 1.14 W/g
Fig. 5(b)	$2b_1 = 6 \text{ nm}$	$f = 150 \text{ kHz}$, SLP = 0.05 W/g
	$2b_1 = 8 \text{ nm}$	$f = 150 \text{ kHz}$, SLP = 0.17 W/g
	$2b_1 = 10 \text{ nm}$	$f = 150 \text{ kHz}$, SLP = 0.69 W/g
	$2b_1 = 12 \text{ nm}$	$f = 150 \text{ kHz}$, SLP = 3.43 W/g
Fig. 6(a)	$2b_1 = 6 \text{ nm}$	$H = 7 \text{ kA/m}$, SLP = 0.05 W/g
	$2b_1 = 8 \text{ nm}$	$H = 7 \text{ kA/m}$, SLP = 0.17 W/g
	$2b_1 = 10 \text{ nm}$	$H = 7 \text{ kA/m}$, SLP = 0.69 W/g
	$2b_1 = 12 \text{ nm}$	$H = 7 \text{ kA/m}$, SLP = 3.43 W/g
Fig. 6(b)	$f = 200 \text{ kHz}$	$H = 7 \text{ kA/m}$, SLP = 0.31 W/g
	$f = 300 \text{ kHz}$	$H = 7 \text{ kA/m}$, SLP = 0.69 W/g
	$f = 350 \text{ kHz}$	$H = 7 \text{ kA/m}$, SLP = 0.94 W/g
	$f = 400 \text{ kHz}$	$H = 7 \text{ kA/m}$, SLP = 1.6 W/g
CASE B (SLP for $N = 60$ magnetic particles in a sphere)		
Fig. 9(a)	$2b_1 = 6 \text{ nm}$	$f = 50 \text{ kHz}$, SLP = 2.79 W/g
	$2b_1 = 8 \text{ nm}$	$f = 50 \text{ kHz}$, SLP = 3.15 W/g
	$2b_1 = 10 \text{ nm}$	$f = 50 \text{ kHz}$, SLP = 3.35 W/g
	$2b_1 = 12 \text{ nm}$	$f = 50 \text{ kHz}$, SLP = 3.48 W/g
Fig. 9(b)	$2b_1 = 6 \text{ nm}$	$f = 17 \text{ kHz}$, SLP = 2.12 W/g
	$2b_1 = 8 \text{ nm}$	$f = 11 \text{ kHz}$, SLP = 2.67 W/g
	$2b_1 = 10 \text{ nm}$	$f = 8 \text{ kHz}$, SLP = 3.04 W/g
	$2b_1 = 12 \text{ nm}$	$f = 5 \text{ kHz}$, SLP = 3.18 W/g
Fig. 9(c)	$H = 7 \text{ kA/m}$	$f = 20 \text{ kHz}$, SLP = 0.82 W/g
	$H = 10 \text{ kA/m}$	$f = 20 \text{ kHz}$, SLP = 1.68 W/g
	$H = 14 \text{ kA/m}$	$f = 20 \text{ kHz}$, SLP = 3.31 W/g
	$H = 18 \text{ kA/m}$	$f = 20 \text{ kHz}$, SLP = 5.47 W/g
Fig. 10(b)	$2b_1 = 6 \text{ nm}$	$H = 7 \text{ kA/m}$, SLP = 0.72 W/g
	$2b_1 = 8 \text{ nm}$	$H = 7 \text{ kA/m}$, SLP = 0.70 W/g
	$2b_1 = 10 \text{ nm}$	$H = 7 \text{ kA/m}$, SLP = 0.84 W/g
	$2b_1 = 12 \text{ nm}$	$H = 7 \text{ kA/m}$, SLP = 0.87 W/g

al. (2002) study [2].

The relaxation time is subject to the aggregate contributions of both Neel and Brownian relaxation forms. Neel relaxation includes the internal rotation of the magnetic moment and also has a characteristic time [22]. Relaxation processes that regulate the heating properties of magnetic nanoparticles are observed.

This study showcases the relationship among the heat generation process with the amplitude and frequency of the applied AC field, the magnetic nanoparticle relaxation processes, and particle size. However, considering that there is a volume gap between the sphere and magnetic particles, magnetic

volume for a sphere-shaped ball with particles depends on a number of particles. As a consequence, SLP also relies on a number of particles and volume gap in a sphere-shaped ball, and his study has been able to demonstrate this.

The current results demonstrate considerable differences in magnetic properties of magnetic particles with the comparable size that are hardly justifiable within present micro-magnetic models of superparamagnetic particles. Reasons for this difference could be a mean particle size, a number of particles, frequency and the amplitude of the exposed field, relaxation time, and volume gap between particles and a sphere-shaped ball.

The most striking result arising from this analysis is that when particles are more close together (less volume gap of a sphere-shaped ball), high SLP is found for the same number of particles in the same sphere-shaped ball with the superparamagnetic situation. These results further help the opinion of dipolar interaction between nanoparticles. In contrast, an experiment carried out by Yadel et al. (2018) [23] had demonstrated that when iron oxide nanoparticles (coated) were well-distributed into the aggregates, the specific absorption rate reached 79% of the value measured for the well-dispersed case. Another experiment by Guibert et al. (2015) [20] (coated and non-coated) observed the role of aggregation of iron oxide nanoparticles on their heating properties by using dynamic light scattering (DLS) and hyperthermia experiments. Their results demonstrate that the SLP of nanoparticles in loose aggregates is compatible with well-dispersed nanoparticles and the arrangement of large and compact aggregates seen by DLS prompts a decline of the SLP. Reciprocal examinations are as yet essential to acquire a more quantitative connection between the degree of the volume gap of a sphere-shaped ball of magnetic particles and the increment of the SLP. Our examination only considers a sphere-shaped ball. In future work, we plan to investigate the impact of different three-dimensional shapes on SLP with loose aggregate and dense aggregate conditions. This finding has significant implications for developing links between heating properties and aggregation. Nevertheless, this investigation will be beneficial for understanding how to regulate the thermal therapies necessitating magnetic hyperthermia treatments.

8. CONCLUSION

The importance of investigating specific loss power for heating applications is apparent, especially in cancer treatment by hyperthermia. A theoretical model has been developed to optimize thermal therapies and calculated parameter dependence for superparamagnetic MNPs (approximative ellipsoid-shaped) within a sphere-shaped ball. The results of this study indicate that when particles are closer together (less volume gap of a sphere-shaped ball), high SLP is found for the same number of particles. This study has found that the influence of a number of particles in a sphere-shaped ball demonstrates that SLP of magnetic particles increases with increasing the number of particles (N), and after $N = 10$ particles, the SLP increment is insignificant. Frequency dependency on SLP of ellipsoid-shaped superparamagnetic nanoparticles is negligible when the frequency is higher than 10 kHz. The Kneedle Algorithm is utilized to estimate the accurate heating efficiency parameter values. These “knees” typically represent valuable points that experimental designers could select to achieve the best balance in inherent tradeoffs between performance and feasibility. In general, therefore, it seems that the SLP of MNPs in a sphere-shaped ball also strongly depends on the magnetic parameters and properties of the particles. This study shows optimal parameter values that have impact on SLP of the accumulation of superparamagnetic nanoparticles (ellipsoid-shaped) into a sphere-shaped ball. In future investigations, it might be possible to develop links between heating properties with loose aggregate and dense aggregate scenarios in the superparamagnetic situation. This work will be most beneficial for understanding how to control the thermal dose using optimal values in therapies necessitating magnetic hyperthermia.

9. APPENDIX

9.1. CASE B

In this section, we illustrate the relationship among particle numbers, sphere volume, and volume gap for different particle diameters ($2b_1 = 6, 8, 10, 12$ nm).

Let us consider a sphere (magnetic ball) with N magnetic particles (Figure 3). The volume of the magnetic ball is $V_{M_2} = 4\pi b_2^3/3$ and N magnetic particles with the $2a_1$, $2b_1$, $2b_1$ axes. The volume gap (V_{gap}) is the volume between sphere and N magnetic particles, shown in Figure 10. Width of a sphere-shaped ball with N particles can be derived from Equation (10), and it depends on the number of magnetic particles (N), width of the magnetic particle (a_1), length/diameter of the magnetic particle (b_1), and volume gap between a sphere and N magnetic particles (V_{gap}).

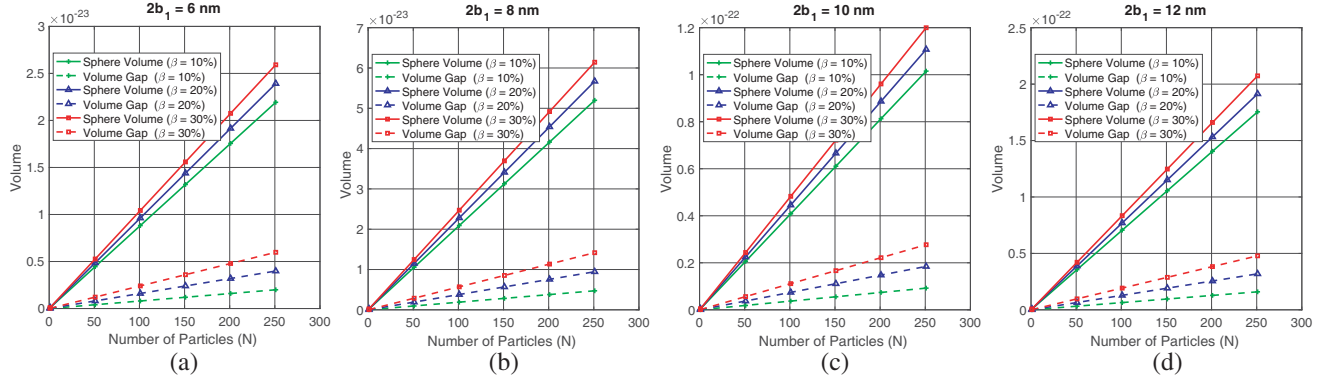


Figure 10. Volume gap (V_{gap}) modelling for Case B (as shown in Figure 3), where $\beta = 10\%$, 20% , 30% . Magnetic particles within a sphere (volume, $V_{M_2} = 4\pi b_2^3/3$) with N magnetic particles ($2a_1$, $2b_1$, $2b_1$ axis) where V_{gap} is volume gap between sphere and N magnetic particles. (a) when $2b_1 = 6$ nm. (b) when $2b_1 = 8$ nm. (c) when $2b_1 = 10$ nm. (d) when $2b_1 = 12$ nm.

ACKNOWLEDGMENT

The first author would like to thank ‘‘CAS President’s International Fellowship Initiative (PIFI)’’ supported by the Chinese Academy of Sciences (CAS), Beijing.

REFERENCES

1. Dennis, C. L. and R. Ivkov, ‘‘Physics of heat generation using magnetic nanoparticles for hyperthermia,’’ *Int. J. Hyperthermia*, Vol. 29, No. 8, 715–729, 2013.
2. Rosensweig, R. E., ‘‘Heating magnetic fluid with alternating magnetic field,’’ *Journal of Magnetism and Magnetic Materials*, Vol. 252, 370–374, 2002.
3. Hergt, R., R. Hiergeist, I. Hilger, W. A. Kaiser, and Y. Lapatnikov, ‘‘Maghemite nanoparticles with very high ac-losses for application in rf-magnetic hyperthermia,’’ *Journal of Magnetism & Magnetic Materials*, Vol. 270, No. 3, 345–357, 2004.
4. Hergt, R. and S. Dutz, ‘‘Magnetic particle hyperthermia - biophysical limitations of a visionary tumour therapy,’’ *Journal of Magnetism and Magnetic Materials*, Vol. 311, 187–192, 2006.
5. Glockl, G., R. Hergt, M. Zeisberger, S. Dutz, S. Nagel, and W. Weitschies, ‘‘The effect of field parameters, nanoparticle properties and immobilization on the specific heating power in magnetic particle hyperthermia,’’ *Journal of Physics Condensed Matter*, Vol. 18, S2935–S2949, 2006.
6. Wang, X., J. Tang, and L. Shi, ‘‘Induction heating of magnetic fluids for hyperthermia treatment,’’ *IEEE Transactions on Magnetics*, Vol. 46, No. 4, 2010.
7. Dutz, S. and R. Hergt, ‘‘Magnetic nanoparticle heating and heat transfer on a microscale: Basic principles, realities and physical limitations of hyperthermia for tumour therapy,’’ *Int. J. Hyperthermia*, Vol. 29, No. 8, 790–800, 2013.
8. Deatsch, A. E. and B. A. Evans, ‘‘Heating efficiency in magnetic nanoparticle hyperthermia,’’ *Journal of Magnetism and Magnetic Materials*, Vol. 354, 163–172, 2014.

9. Noh, S., S. Moon, T. Shin, Y. Lim, and J. Cheon, "Recent advances of magneto-thermal capabilities of nanoparticles: From design principles to biomedical applications," *Nanotoday*, Vol. 13, 61–76, April 2017.
10. Saucier, R., "Shape factor modeling and simulation," US Army Research Laboratory, Tech. Rep. ARL-TR-7707, June 2016.
11. Golneshan, A. A. and M. Lahonian, "The effect of magnetic nanoparticle dispersion on temperature distribution in a spherical tissue in magnetic fluid hyperthermia using the lattice boltzmann method," *Int. J. Hyperthermia*, Vol. 27, No. 3, 266–274, May 2011.
12. Moise, S., E. Céspedes, D. Soukup, J. Byrne, A. E. Haj, and N. Telling, "The cellular magnetic response and biocompatibility of biogenic zinc- and cobalt-doped magnetite nanoparticles," *Nature Scientific Reports*, Vol. 7, 1–11, 2017.
13. Neel, L., "Influence des fluctuations thermiques a l'aimantation des particules ferromagnetiques," *C. R. Acad. Science*, Vol. 228, 664–668, 1949.
14. Frenkel, J., *The Kinetic Theory of Liquids*, Dover Publications, New York, 1955.
15. Delaunay, L., S. Neveu, G. Noyel, and J. Monin, "A new spectrometric method, using a magneto-optical effect, to study magnetic liquids," *Journal of Magnetism and Magnetic Materials*, Vol. 149, No. 3, 239–249, September 1995.
16. Landau, L. D. and E. M. Lifshitz, *Electrodynamics of Continuous Media*, Pergamon Press, London, 1960.
17. Satopaa, V., J. Albrecht, and D. Irwin, "Finding a "kneedle" in a haystack: Detecting knee points in system behavior," *International Conference on Distributed Computing Systems Workshops (ICDCSW)*, June 2011.
18. Muller, R., S. Dutz, A. Neeb, A. C. B. Catob, and M. Zeisberger, "Magnetic heating effect of nanoparticles with different sizes and size distributions," *Journal of Magnetism and Magnetic Materials*, Vol. 328, 80–85, 2013.
19. Fantechi, E., C. Innocenti, M. Albino, E. Lottini, and C. Sangregorio, "Influence of cobalt doping on the hyperthermic efficiency of magnetite nanoparticles," *Journal of Magnetism and Magnetic Materials*, Vol. 380, 265–271, 2015.
20. Guibert, C., V. Dupuis, V. Peyre, and J. Fresnais, "Hyperthermia of magnetic nanoparticles: Experimental study of the role of aggregation," *J. Phys. Chem. C*, Vol. 119, No. 50, 28 148–28 154, 2015.
21. Butler, R., "Theoretical single-domain grain size range in magnetite and titanomagnetite," *Journal of Geophysical Research Atmospheres*, Vol. 80, No. 29, 4049–4058, 1975.
22. Abenojar, E., S. Wickramasinghe, J. Bas-Concepcion, and A. Samia, "Structural effects on the magnetic hyperthermia properties of iron oxide nanoparticles," *Progress in Natural Science: Materials International*, Vol. 26, No. 5, 440–448, October 2016.
23. Yadel, C., A. Michel, S. Casale, and J. Fresnais, "Hyperthermia efficiency of magnetic nanoparticles in dense aggregates of cerium oxide/iron oxide nanoparticles," *Appl. Sci.*, Vol. 8, 1241, 2018.